Annals of Biomedical Engineering, Vol. 33, No. 4, April 2005 (© 2005) pp. 444–456
DOI: 10.1007/s10439-005-2499-y

Computational Study of Fluid Mechanical Disturbance Induced by Endovascular Stents

TAEWON SEO,[1,2] LEVANTO G. SCHACHTER,[1] and ABDUL I. BARAKAT[1]

[1]Department of Mechanical and Aeronautical Engineering, University of California, Davis, CA and [2]School of Mechanical Engineering, Andong National University, Andong, South Korea

(Received 20 July 2004; accepted 3 November 2004)

Abstract—Arterial restenosis following stent deployment may be influenced by the local flow environment within and around the stent. We have used computational fluid dynamics to investigate the flow field in the vicinity of model stents positioned within straight and curved vessels. Our simulations have revealed the presence of flow separation and recirculation immediately downstream of stents. In steady flow within straight vessels, the extent of flow disturbance downstream of the stent increases with both Reynolds number and stent wire thickness but is relatively insensitive to stent interwire spacing. In curved vessels, flow disturbance downstream of the stent occurs along both the inner and outer vessel walls with the extent of disturbance dependent on the angle of vessel curvature. In pulsatile flow, the regions of flow disturbance periodically increase and decrease in size. Non-Newtonian fluid properties lead to a modest reduction in flow disturbance downstream of the stent. In more realistic stent geometries such as stents modeled as spirals or as intertwined rings, the nature of stent-induced flow disturbance is exquisitely sensitive to stent design. These results provide an understanding of the flow physics in the vicinity of stents and suggest strategies for stent design optimization to minimize flow disturbance.

Keywords—Restenosis, Flow separation, Flow recirculation, Intravascular devices, CFD, Atherosclerosis, Intimal hyperplasia.

INTRODUCTION

Endovascular stents are expandable wire-mesh structures that were developed to minimize the incidence of restenosis following balloon angioplasty. Restenosis is a complex and incompletely understood process in which arterial occlusion redevelops over a period of several months following angioplasty. Stents are deployed in a compressed state and are expanded at the stenosis site to both improve overall patency of the arterial lumen and provide structural stability to the vascular wall. Several studies have demonstrated that stents have indeed reduced restenosis rates significantly, from 30 to 50% of all angioplasty procedures to 20–35%.[37] More recently, the development of drug-eluting stents appears to have further reduced the incidence of restenosis; however, experience with these stents remains limited, and restenosis continues to occur in some of the cases.[26,27] The persistence of the occurrence of restenosis even in the presence of stents emphasizes the need for a better understanding of factors contributing to restenosis.

Placement of a stent within an arterial segment causes local injury to the vascular endothelium, the cellular monolayer lining the inner surfaces of blood vessels. Furthermore, overexpansion of stents, which occurs commonly, may lead to subendothelial and medial damage. This damage as well as the presence of the stent itself stimulate rapid thrombotic responses that likely contribute to the complex signaling cascades involved in the development of the intimal hyperplasia central to the occurrence of in-stent restenosis.[7,34] Indeed, several studies have demonstrated that vigorous antithrombotic therapy and the use of heparin-coated stents considerably reduce the incidence of restenosis.[16,28] Concomitant with the thrombotic reaction, endothelial cells in the vicinity of the injured area rapidly migrate and proliferate in a normal wound healing response aimed at reestablishing a continuous endothelial monolayer. There is evidence that the success of a stenting procedure depends centrally on a sufficiently rapid rate of reendothelialization following the injury induced by stent deployment.[9,17,35]

The extent of thrombosis in the vicinity of an implanted stent and the level of platelet activation within thrombi are likely affected by the local flow environment.[7,22] Furthermore, *in vitro* studies have demonstrated that endothelial cell migration rates are not only affected by flow but are also sensitive to the type of flow to which the cells are exposed.[1,15] More specifically, endothelial migration appears to be especially slow in regions of relatively large spatial gradients of shear stress, as might occur around points of boundary layer separation and reattachment.[15] If similar behavior occurs *in vivo*, then the rate of reendothelialization in the vicinity of a stent would be expected to depend on local hemodynamics. More generally, shear stress is

Address correspondence to Abdul I. Barakat, Professor, Department of Mechanical and Aeronautical Engineering, University of California, One Shields Avenue, Davis, CA 95616. Electronic mail: abarakat@ucdavis.edu

0090-6964/05/0400-0444/1 © 2005 Biomedical Engineering Society

known to intricately regulate endothelial cell structure and function[4,14,31] and to play a role in both the localization of early atherosclerotic lesions[23,25,29] and the formation of neointimal tissue in vascular grafts.[32] Therefore, a possible role for shear stress in the process of instent restenosis appears plausible.

Relatively little is known about the fluid dynamic environment in the vicinity of endovascular stents. An issue of central interest in the present study is the extent of fluid dynamic disturbance induced by the placement of a stent within an arterial segment. Berry *et al.*[7] used a combination of flow visualization experiments and computational fluid dynamics (CFD) to demonstrate that the struts of a stent disturb the flow sufficiently to lead to regions of flow separation and weak recirculation in the regions between the struts. Wentzel *et al.*[38] imaged the three-dimensional geometry of stented pig coronary arteries and demonstrated significantly altered curvature relative to unstented vessels. Subsequent CFD simulations revealed that the stent-induced changes in vessel curvature led to alterations in the shear stress distribution at the stent edges. More recently, Wentzel *et al.*[37] tracked the development of intimal hyperplasia in stented patients and combined this information with CFD simulations to conclude that neointimal thickness is inversely related to the magnitude of wall shear stress. The current state of the art in our understanding of the potential implications of fluid mechanics to stent design has recently been reviewed.[18]

The purpose of the present computational study is to investigate the extent of fluid mechanical disturbance induced by the presence of a stent within straight and curved arterial segments under both steady and pulsatile flow conditions. Of particular interest is the development of a fundamental understanding of the effect of stent design, vessel geometry, and the prevailing flow conditions on flow separation zones in the vicinity of an endovascular stent. The possible implications of the results for stent design optimization are discussed.

COMPUTATIONAL METHODS

Stent and Flow Modeling

The models used in most of the computations are depicted in Fig. 1. In these simulations, the stent wires are idealized as a series of circular rings of diameter d and interring spacing w. The model stent is placed within either a straight or a curved arterial segment of uniform diameter D. Both the stent wires and the arterial wall are assumed rigid. In the straight vessel geometries, most simulations are performed with vessel segments 2D long both upstream and downstream of the model stent [Fig. 1(A)]. In the case of the curved vessel simulations, where the stent is positioned immediately past the curvature, the radius of curvature is 2D and vessel lengths of 2D are typically assumed upstream of the curvature and downstream of the stent for most simulations [Fig. 1(B)]. To probe the sensitivity of the simulation results to the length of vessel segment simulated, computations with larger vessel lengths downstream of the stent (5D) have also been performed and have been shown to lead to flow patterns in the stent region that are virtually identical to those obtained with vessel lengths of 2D. Due to axisymmetry, the straight vessel simulations are two-dimensional, while the curved vessel computations are fully three-dimensional. Both steady and pulsatile flow simulations are performed. In the unsteady flow computations, flow pulsatility is idealized as a nonreversing sinusoid with a physiological frequency of 1 Hz. The simulations often revealed the presence of a flow separation and weak recirculation zone immediately downstream of the model stent. The length of this recirculation zone is denoted by L [Fig. 1(A)] and is a parameter of primary interest in the present study.

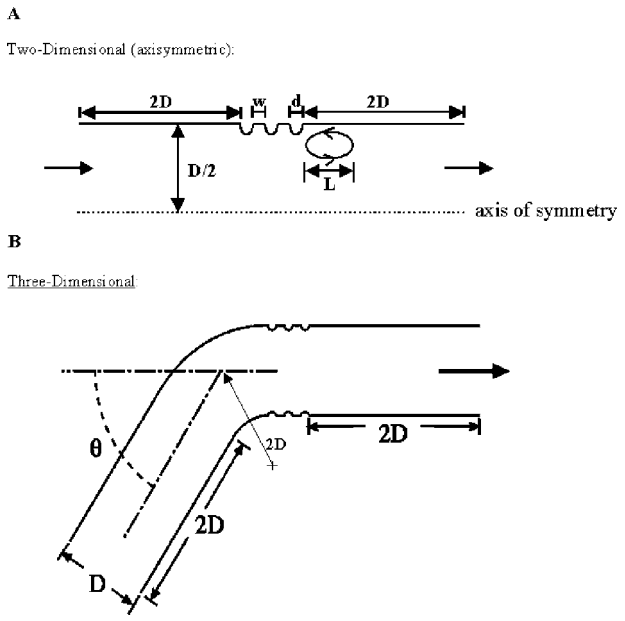

FIGURE 1. Geometric models used in the simulations. The model stent, idealized as a series of parallel circular rings of diameter *d* and spacing *w*, is positioned orthogonal to the vessel axis. The vessel diameter is *D* and the length of the flow separation zone immediately downstream of the stent is denoted by *L*. (A) Two-dimensional (axisymmetric) models for straight vessel segments. (B) Three-dimensional models for curved vessel segments. θ denotes the angle of curvature. The radius of curvature is 2D.

Governing Equations and Solution Method

The governing equations are the conservation of mass and linear momentum which, cast in integral (control volume) formulation for an incompressible fluid, are given by:

$$\text{Mass}: \quad \int\int_A (\vec{v} \cdot \vec{n})\, dA = 0 \tag{1}$$

$$\text{Linear Momentum}: \frac{\partial}{\partial t}\int\limits_V\!\!\int\!\!\int \rho\vec{\mathrm{v}}\,dV + \int\limits_A\!\!\int \rho\vec{\mathrm{v}}(\vec{\mathrm{v}}\cdot\vec{n})\,dA$$

$$= -\int\limits_A\!\!\int p\vec{n}\,dA + \int\limits_A\!\!\int \underline{\underline{\tau}}\cdot\vec{n}\,dA \qquad (2)$$

where ρ is the fluid density, $\vec{\mathrm{v}}$ is the fluid velocity vector, $\vec{n}$ is the unit outward normal vector, dA is a differential area, dV is a differential volume, p is the fluid pressure, and $\underline{\underline{\tau}}$ is the fluid viscous stress tensor.

Blood behaves as a Newtonian fluid for shear rates greater than $\sim$100 s^{-1}.[13] Shear rates in large arteries are generally considerably larger than this value;[5,23,25,30] therefore, most simulations in the present study assume the fluid to be Newtonian. Under this assumption, Eqs. (1) and (2) reduce to the Navier-Stokes equations. However, regions of flow separation and recirculation, as might be expected to occur downstream of sharp changes in vessel curvature, are often characterized by very small shear rates; therefore, limited simulations were performed using a non-Newtonian model for blood flow. In this case, blood dynamic viscosity was given by the Carreau model:

$$\mu = \mu_\infty + (\mu_\mathrm{o} - \mu_\infty)[1 + (\lambda\dot{S})^2]^{(n-1)/2} \qquad (3)$$

where μ is the dynamic viscosity of blood, μ_∞ and μ_o are the values of the viscosity as the shear rate goes to infinity and zero, respectively, λ is the time constant associated with the viscosity changes with shear rate, $\dot{S}$ is the shear rate, and n is the power law index. The following Carreau model values were used in the present simulations: $\mu_\infty =$ 0.0035 kg/m-s, $\mu_\mathrm{o} = 0.25$ kg/m-s, $\lambda = 25.00$s, and $n =$ 0.25. These values were determined from a best fit of the model in Eq. (3) to the experimental findings of Chien *et al.*[13] obtained using whole blood over shear rates ranging from 0.01 to 50 s^{-1}.

Equations (1) and (2) were solved subject to the following boundary conditions: no slip (zero velocity) on all walls, a prescribed velocity profile (either uniform or parabolic) at the flow inlet, and zero pressure at the flow outlet. To test the sensitivity of the results to the boundary condition at the flow outlet, limited simulations were performed using a fully developed flow profile (i.e. $\partial\vec{\mathrm{v}}/\partial\vec{n} = 0$), and the results were compared to those with a zero pressure outlet. The results of this comparison have established that under the conditions studied, the flow field in the vicinity of the model stent is insensitive to the outlet boundary condition.

The governing equations were solved using the commercial computational fluid dynamic code FLUENT (version 5, Fluent Inc., Lebanon, NH). FLUENT is a finite-volume code in which the flow equations are discretized for each cell in the system. The linearized first order equations are then solved implicitly using the point Gauss-Seidel scheme. Unstructured meshes with tetrahedral cells were used in all simulations. For the two-dimensional simulations, the meshes ranged from 16,288 to 99,492 nodes; the equivalent range for the three-dimensional simulations was 159,576 to 1,266,060. Figure 2 illustrates typical computational meshes used in the straight and curved vessel simulations and demonstrates the higher mesh density in the vicinity of the model stent.

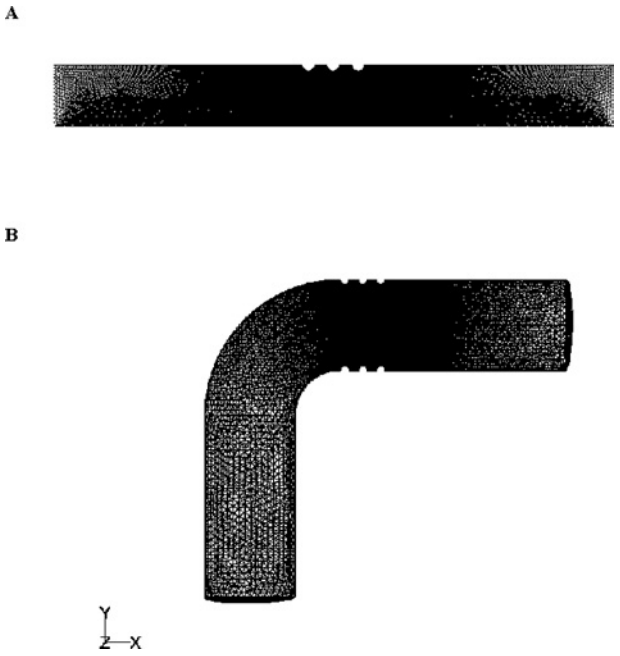

FIGURE 2. Typical computational meshes used in the straight (A) and curved (B) vessel simulations. Note the higher mesh density in the vicinity of the model stent.

FLUENT's numerical solutions were validated extensively against experimental data obtained for flow over a backward facing step for Re in the range 100–400.[2] This comparison has demonstrated that FLUENT is able to accurately reproduce the experimental findings. More specifically, the difference between the numerical predictions and the experimental results in the size of the flow recirculation zone downstream of the step for the different values of Re ranged from 0.4 to 8% (data not shown). The equivalent difference in peak velocity downstream of the step ranged from 3 to 9.5% (data not shown). Given the inherent uncertainties in experimental velocity measurement, these results provide confidence in the accuracy of FLUENT's numerical predictions.

All simulations were performed using either a 450 MHz Pentium III (512 MB of RAM) or a 1.2-GHz Athlon Thunderbird (1.28 GB of RAM) personal computer running Windows NT. In steady flow convergence was based on the residual in continuity and the three velocity components dropping below prescribed values (typically 10^{-5} for continuity and 10^{-7} for the velocity components); this was always achieved within 500 iterations for the smallest simulations and within 8000 iterations for the largest ones. In unsteady flow, convergence for each time step was based

on the residual in continuity falling below a prescribed value (typically 10^{-5}). Time-periodic solutions were typically obtained within 4–5 cycles and were defined when the cycle-average difference in the size of the flow separation zone immediately downstream of the stent between two successive cycles fell below 5%. Under those conditions, differences in velocities between successive cycles were smaller than 1%. All solutions presented have been verified to be mesh-independent—increasing the mesh density by 5–10% yields velocities that are within 1% of those shown here and flow separation zone lengths that are within 2% of those given.

Range of Parameters Studied and Quantities of Primary Interest

In all the simulations the vessel diameter D was assumed to be 4 mm, a representative value for portions of the human coronary tree within which stents are usually deployed.[3] The fluid was assumed to have a density $\rho = 1060$ kg/m^3 and a dynamic viscosity $\mu = 0.0035$ kg/m-s (for the Newtonian flow simulations). Curved vessel simulations were performed for angles of curvature [θ in Fig. 1(B)] of 30°, 60°, and 90°. The flow Reynolds numbers (Re) based on vessel diameter (D) and mean axial velocity at the flow inlet ($Re = \rho v_{\text{in}} D/\mu$) were typical of those encountered within coronary arteries and ranged from 100 to 800. To assess the sensitivity of the flow field to variations in stent geometry, both stent wire thickness (d) and stent interwire spacing (w) were varied over a wide range—dimensionless wire thickness (d/D) ranged from 0.05 to 0.3 and dimensionless interwire spacing (w/D) ranged from 0 to 0.3. In addition, the number of wires making up the stent was varied from 1 to 7. Finally, simulations were performed on more realistic stent configurations in which the stent wires crossed and intertwined. In the pulsatile flow simulations, a 1-Hz nonreversing sinusoidal velocity was imposed at the flow inlet as follows:

$$v_{\text{in}}(t) = v_{\text{o}}\,(1 + 0.5 \sin 2\pi t)\,, \tag{4}$$

where v_o is the cycle-average inlet velocity. The corresponding Womersley number based on the vessel radius is 2.8.

A parameter of primary interest in the present simulations was the extent of fluid mechanical disturbance induced by the model stent. To quantify this disturbance, we have focused on the impact of various flow and geometric parameters on the size of the flow separation and recirculation zone immediately downstream of the stent (L in Fig. 1A). One rationale for paying particular attention to this region is that the wall shear stress within flow recirculation zones is typically quite low, and regions of low shear stress have been implicated in the development of neointimal growth following stent implantation.[37] A very small region of flow separation and recirculation was also observed immediately upstream of the stent; however, the size of this disturbed flow zone was considerably smaller than that downstream of the stent. The length of the flow recirculation zone L was determined as the distance between flow separation and reattachment points downstream of the stent. This could be accurately computed by determining the spacing between the two points downstream of the stent where the wall shear stress (or shear rate) based on the axial flow velocity passed through zero. Another quantity of interest in the present simulations is the total wall shear stress (τ_w), which is defined as:

$$\tau_w = \mu \left(\frac{\partial u_j}{\partial x_i} + \frac{\partial u_i}{\partial x_j} \right) \Bigg|_{\text{wall}} . \tag{5}$$

RESULTS

Steady Flow in Straight Vessels

Initial simulations focused on steady Newtonian flow in straight vessel segments [Fig. 1(A)]. As already described, the majority of these simulations were two-dimensional due to axisymmetry. To verify the validity of the axisymmetric flow assumption, a limited number of fully three-dimensional simulations were performed and were shown to lead to identical results to those obtained in the axisymmetric simulations. An initial difficulty in the modeling was the need to establish the minimum stent length that needed to be modeled in order to fully capture the physics of the flow disturbance induced by the stent. Therefore, a series of simulations was performed to probe the sensitivity of the size of the flow separation zone downstream of the stent to the number of wires making up the stent. The results of these simulations demonstrated that for Re ranging from 200 to 800, the size of the flow recirculation zone downstream of the stent was largest for a one-wire stent and decreased slightly as the number of stent wires was increased from one to three (data not shown). An additional increase in the number of stent wires did not cause a further decrease in the size of the flow recirculation zone. These results demonstrate a level of fluid mechanical interaction among the stent wires and suggest that while the velocity profile approaching the second stent wire is altered considerably due to the presence of the first stent wire, the extent of this alteration becomes asymptotically smaller for subsequent stent wires. The results also indicate that if the parameter of primary interest is the flow recirculation region downstream of the stent, then a three-wire stent provides an adequate model for capturing the necessary flow physics. Therefore, most of the subsequent simulations were performed with a three-wire stent.

Figure 3(A) depicts the dependence of the dimensionless length of the flow separation and recirculation zone immediately downstream of a three-wire model stent (L/D) on the dimensionless stent wire thickness (d/D) for Re in the range 200–800 and for a uniform velocity profile at the

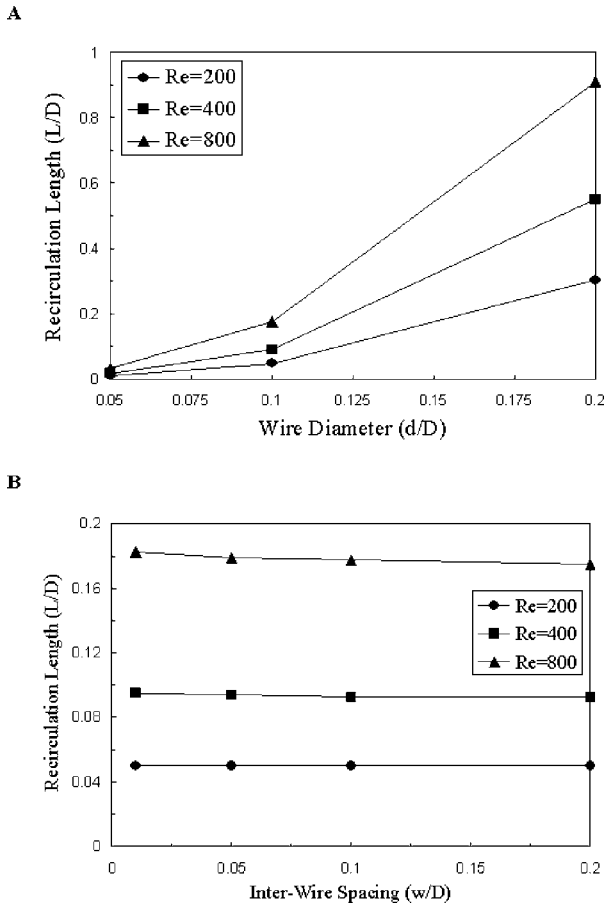

FIGURE 3. Impact of stent geometry on the size of the flow separation zone immediately downstream of a three-wire stent positioned within a straight arterial segment. Flow is steady with *Re* in the range 200–800. (A) Effect of stent wire thickness (*d*/*D*) for *w*/*D* = 0.1. (B) Effect of stent interwire spacing (*w*/*D*) for *d*/*D* = 0.1.

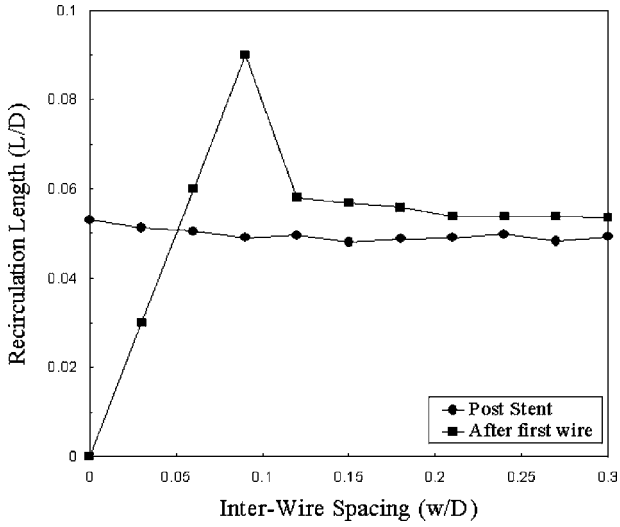

FIGURE 4. Effect of stent interwire spacing (*w*/*D*) on the sizes of flow separation zones both within and downstream of a two-wire stent positioned within a straight arterial segment. Flow is steady with a *Re* = 800 and *d*/*D* = 0.06. The sizes of the flow separation zone between the two stent wires and that immediately downstream of the stent are shown separately.

flow inlet. The results demonstrate that for a given value of d/D, L/D increases nearly linearly with Re. This increase is not surprising as higher Re flows are associated with higher inertial effects that tend to promote flow separation. At a given Re, L/D increases rapidly with d/D, suggesting that thicker-wire stents lead to increased flow disturbance downstream of the stent.

Figure 3(B) illustrates that for Re in the range 200–800, the size of the recirculation flow zone downstream of the stent is virtually insensitive to the interwire spacing (expressed in dimensionless terms as w/D) over a wide range of this spacing ($0.01 \leq w/D \leq 0.2$). It should be emphasized that this conclusion applies strictly to the flow disturbance downstream of the stent. Naturally, flow disturbance in between stent wires is a strong function of the interwire spacing. This is more clearly illustrated in Fig. 4 which separately depicts the size of the flow separation and recirculation zone downstream of the first wire and that downstream of the second wire as a function of w/D for a two-wire stent with $d/D = 0.06$ and $Re = 800$. Consistent with Fig. 3(B), L/D downstream of the second wire is a very weak function of w/D. On the other hand, L/D between the two wires (i.e. downstream of the first wire) exhibits three distinct types of behavior. The first occurs at small w/D ($w/D \leq 0.09$) where a single slowly rotating recirculation zone is observed between the two wires and where L/D increases with interwire spacing with a slope of one, indicating that the flow recirculation zone occupies the entire spacing between the wires. The second type of behavior occurs for $0.09 \leq w/D \leq 0.12$ where L/D decreases with w/D. In this zone, two distinct flow recirculation zones are present between the two wires (one downstream of the first wire and the other upstream of the second wire), and the wires are sufficiently close together so that the presence of the second wire impacts the flow disturbance downstream of the first wire. Finally, at relatively large w/D ($w/D > 0.12$), the wires are sufficiently far apart so that the fluid mechanical interactions are limited, and L/D becomes virtually independent of w/D [similar to Fig. 3(B)].

There is mounting evidence that the most relevant fluid mechanical parameter in the regulation of vascular cell biology is the shear stress (and gradients, both spatial and temporal, of shear stress) to which the cells are exposed.[15,31,39] Figure 5 illustrates the wall shear stress [defined in Eq. (5)] distribution as a function of the axial distance for an arterial segment containing a three-wire stent and for flow Re in the range 200–800. These simulations were performed under the conditions of $d/D = w/D = 0.1$ and a uniform velocity profile at the vessel inlet. The wall shear stress is relatively flat upstream of the stent ($x/D < 0$), and, as expected, it goes to zero at the upstream end of the stent

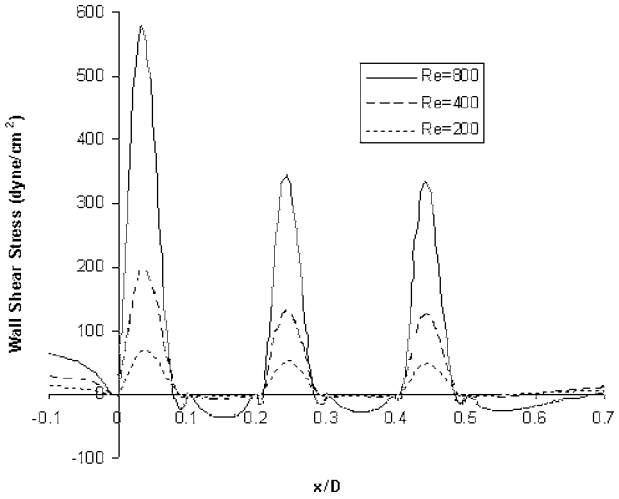

FIGURE 5. Wall shear stress distribution for a straight vessel segment within which a three-wire stent has been positioned. The portion of the vessel shown corresponds to a region shortly upstream of ($x/D < 0$), within ($0 \le x/D \le 0.5$), and shortly downstream of ($x/D > 0.5$) the model stent. Flow is steady with *Re* in the range 200–800 and $d/D = w/D = 0.1$.

($x/D = 0$). The wall shear stress distribution exhibits pronounced peaks as the fluid passes over the three stent wires, and the amplitude of these peaks increases with *Re*. In the regions between the wires and immediately downstream of the stent, the wall shear stresses are relatively low and negative due to flow separation and weak recirculation in those areas. Interestingly, at $Re = 800$, each of the recirculation zones between the stent wires breaks up into small recirculation cells immediately adjacent to the wires that are interspersed by a larger recirculation cell.

All the simulations described thus far were performed with a uniform inlet velocity profile. *In vivo*, complex arterial geometry often leads to a variety of different velocity profiles;[5,12,25] therefore, to investigate the possible impact of the inlet velocity profile on flow disturbance downstream of stents, we have performed simulations with a parabolic inlet profile. The results demonstrate that for a three-wire stent in a straight vessel segment with $d/D = 0.1$ and $w/D = 0.1$, the size of the recirculation flow zone downstream of the stent is virtually insensitive to the inlet velocity profile for $Re = 200$, while for $Re = 400$ or 800, the recirculation zone is slightly (7–8%) smaller for the parabolic inlet profile than that obtained with the uniform inlet profile (data not shown). Another consideration relates to the fact that the results shown in Fig. 3 were obtained with the standard vessel lengths of 2D both upstream and downstream of the stent [Fig. 1(A)]. We have verified that increasing the downstream vessel length to a length of 5D has virtually no impact on the results (data not shown). This suggests that for the flow conditions considered, the imposed boundary condition at the flow outlet does not affect the flow field in the vicinity of the stent.

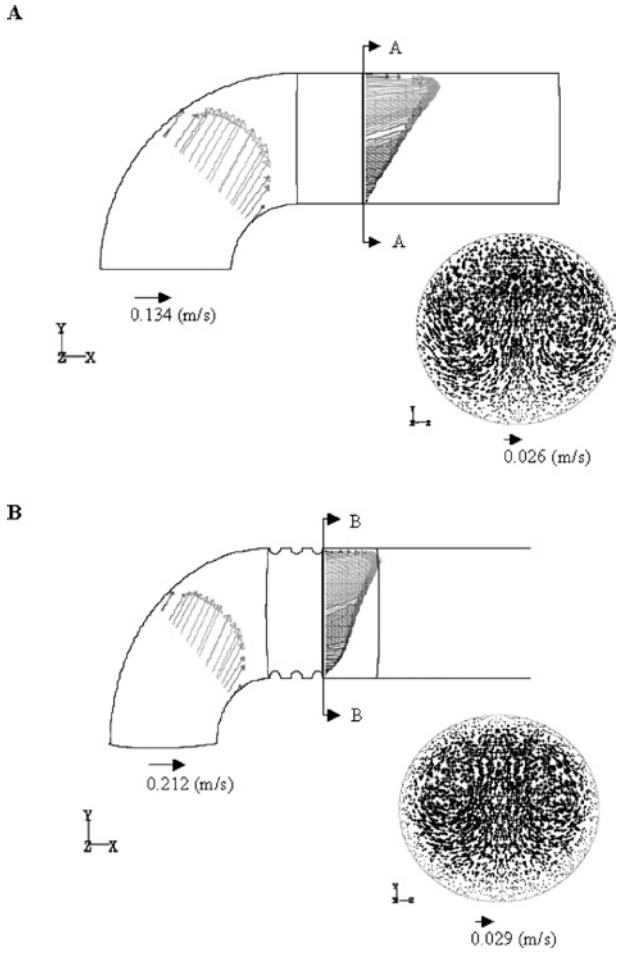

FIGURE 6. Velocity vectors within a 90° curved vessel for steady flow at *Re* = 400 in the absence (A) and presence (B) of a model stent. Also shown are secondary flow velocities immediately downstream of the curvature (sections A-A and B-B).

Steady Flow in Curved Vessels

The simulations thus far have been confined to straight arterial segments. The coronary vasculature within which stents are commonly deployed exhibits a highly complex geometry with extensive curvature.[3] We have extended our simulations to three-dimensional models of curved vessels having different angles of curvature and within which model stents were positioned immediately downstream of the vessel curvature (Fig. 1B). Consistent with previous studies,[6,8–10,30] our simulations of flow in curved vessels without stents demonstrate that centrifugal forces lead to skewness of the velocity profile toward the outer wall of the curvature, leading to flow separation along the inner wall [Fig. 6(A)]. In the presence of a stent, the skewness of the velocity profile toward the outer vessel wall persists, and flow separation and recirculation zones are observed downstream of the stent along both the inner and outer walls of the curved vessel [Fig. 6(B)]. Although these zones appeared to be closed recirculation zones in the plane of symmetry (i.e.,

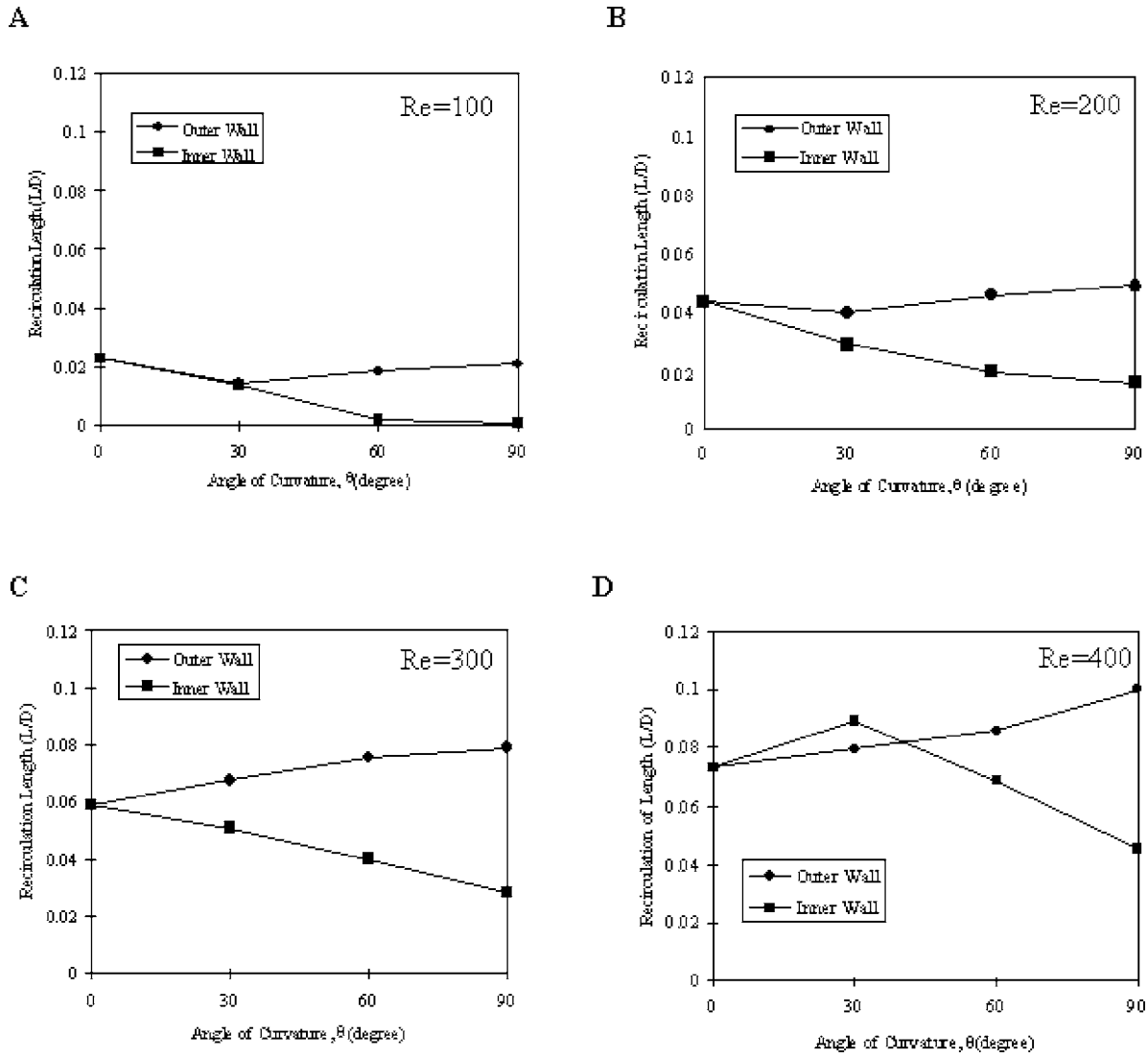

FIGURE 7. Impact of vessel curvature on the size of the flow separation zone immediately downstream of a three-wire stent positioned within a curved arterial segment for different values of *Re*. The flow separation zones along the inner and outer walls are shown separately. Flow is steady with $d/D = w/D = 0.1$.

plane of curvature), this was not the case outside this plane. For instance, along the vessel side walls, flow recirculation took the form of slowly looping streamlines that eventually exited the recirculation zones and proceeded downstream. The figure also depicts inplane velocities downstream of the curvature (sections A-A and B-B) demonstrating the secondary flow patterns within the vessel cross-section. It is observed that the intensity of these secondary flows is considerably larger in the presence of the stent—the peak transverse velocities in the presence of the stent are approximately twice as large as those in the case without a stent.

Figure 7 depicts the sizes of the flow separation zones (L/D) along both the inner and outer walls in the plane of symmetry as a function of the angle of curvature θ for four values of the flow *Re*. For all values of *Re* studied, the relative sizes of the flow separation zones along the inner and outer walls depend intricately on θ. More specifically, the flow separation region is for the most part (all cases with the exception of $\theta = 30^\circ$ at $Re = 400$) larger along the outer wall than along the inner wall. This can be explained by the fact that the fluid along the inner wall has less momentum than that along the outer wall and hence is less likely to undergo separation as it flows over the stent. Furthermore, the size of the flow separation region increases with increased curvature along the outer wall but decreases with curvature along the inner wall. This is attributable to the fact that the fluid momentum shift toward the outer wall increases with curvature. These results suggest that the presence of a stent qualitatively alters the structure of the flow field within a curved vessel and that the detailed character of this alteration depends on both the extent of vessel curvature and the flow *Re*. Our results have also

demonstrated that even when the flow separation zones along both the inner and outer walls have comparable sizes, the skewness of the velocity profile toward the outer vessel wall leads to a situation where the spatial gradients in shear stress are considerably larger along the outer wall than along the inner wall (data not shown).

Pulsatile Flow in Straight and Curved Vessels

Although the steady flow results described thus far provide valuable insight into the fluid mechanics in the vicinity of endovascular stents, the physiological significance of steady flow simulations is limited. We have extended the computations to unsteady flow in which flow pulsatility has been idealized as a nonreversing sinusoid of the form given in Eq. (4). All pulsatile flow results shown correspond to the time-periodic solution, which was typically achieved within 4–5 pulsatile cycles. In straight vessels, flow pulsatility leads to the periodic increase and decrease in the size of the disturbed flow separation zones both within and downstream of the stent. The behavior of flow disturbance downstream of the stent during the course of the 1-s pulsatile cycle is depicted in Fig. 8 for the case of a three-wire stent with $d/D = w/D = 0.1$ and cycle-mean $Re = 200$. The results demonstrate that, despite a slight phase lag ($\sim 30^\circ$), the temporal evolution of the flow separation zone downstream of the stent closely mirrors that of the inlet velocity waveform. Furthermore, the maximum size of the flow separation zone downstream of the stent during the pulsatile cycle matches that obtained for steady flow at a Re equivalent to the peak Re during the cycle [$Re = 300$; see Fig. 3(A)]. The pulsatile flow simulations additionally

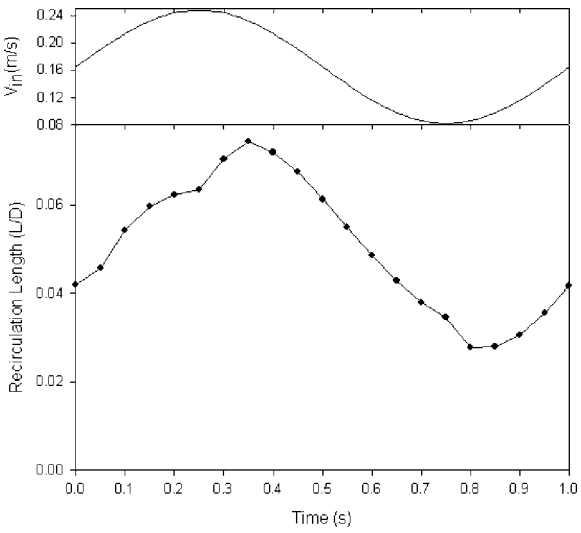

FIGURE 8. Time evolution of the size of the flow separation zone immediately downstream of a three-wire stent positioned within a straight arterial segment during the course of a 1-Hz sinusoidal pulsatile cycle. The cycle-average flow $Re = 200$ and $d/D = w/D = 0.1$.

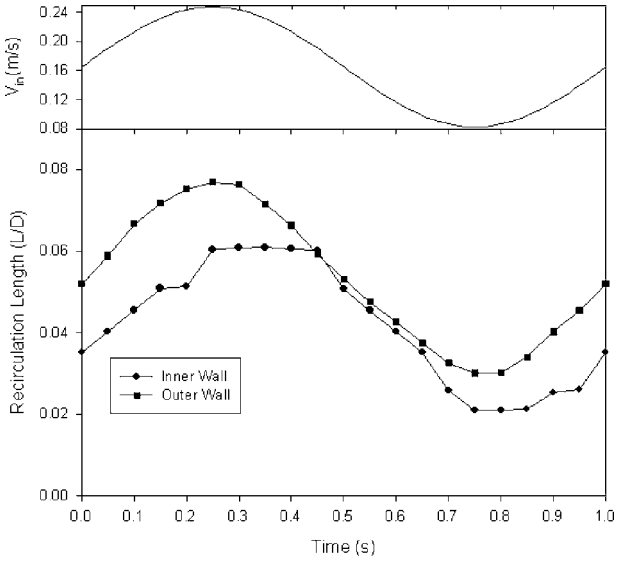

FIGURE 9. Time evolution of the size of the flow separation zone immediately downstream of a three-wire stent positioned within a 60° curved arterial segment during the course of a 1-Hz sinusoidal pulsatile cycle. The flow separation zones along the inner and outer walls are shown separately. The cycle-average flow $Re = 200$ and $d/D = w/D = 0.1$. The top portion of the figure depicts the sinusoidal variation of inlet velocity.

demonstrate that the flow separation zones in the region between the stent wires also periodically increase and decrease in size (data not shown). These results demonstrate the need to include flow unsteadiness in the simulations and suggest that in pulsatile flow, the character of stent-induced flow disturbance is highly dynamic.

Figure 9 illustrates the evolution during the pulsatile cycle of the flow separation and recirculation zones along the inner and outer walls of a 60° curved arterial segment with a mean $Re = 200$. These simulations were performed using a three-wire stent with $d/D = w/D = 0.1$. The results demonstrate that the size of the flow separation zone along each of the two walls periodically increases and decreases in size. Furthermore, similar to the steady flow results (Fig. 7), the separation zone along the outer wall of the curved vessel is larger than that along the inner wall throughout the pulsatile cycle.

Effect of Non-Newtonian Fluid Properties

Blood exhibits prominent non-Newtonian behavior at shear rates smaller than $\sim 100\ s^{-1}$.[13] Because shear rates within flow recirculation zones are typically small, we investigated the impact of the non-Newtonian properties of blood on the flow separation zones downstream of stents under conditions of steady flow in straight vessel segments. The non-Newtonian behavior of blood was determined by fitting the experimental data of Chien *et al.*[13] to the Carreau model given in Eq. (3) as illustrated in Fig. 10(A). Figure 10(B) depicts the wall shear stress computed for a three-wire stent with $d/D = w/D = 0.1$ and a $Re = 400$

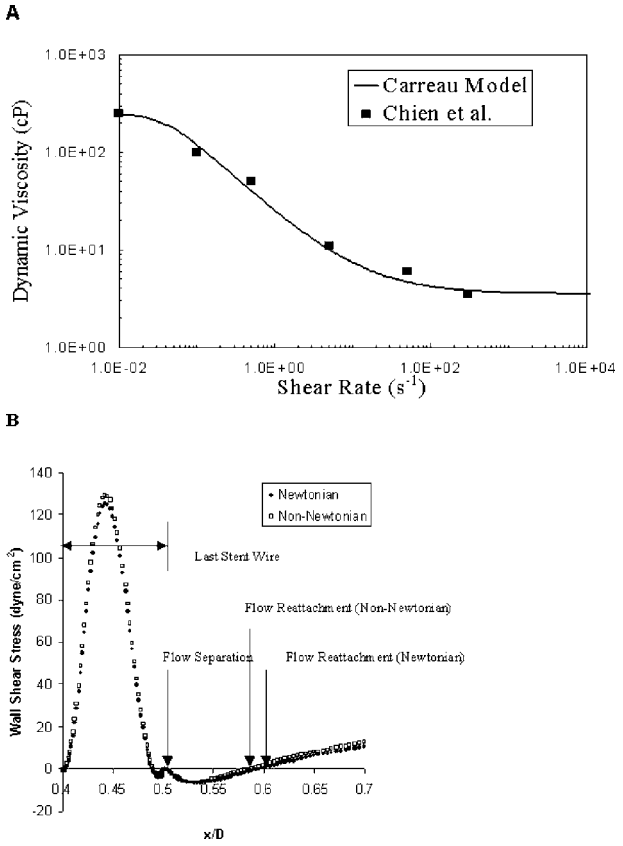

FIGURE 10. (A) Carreau model used to describe the non-Newtonian behavior of blood. The model parameters are obtained by fitting the Carreau equation to the experimental results of Chien *et al.*[13] (B) Effect of non-Newtonian fluid properties on the wall shear stress in a vessel within which a three-wire stent is positioned. Shown is the portion of the vessel wall corresponding to the last stent wire as well as the region immediately downstream of the stent. Flow is steady with $Re = 400$ and $d/D = w/D = 0.1$. Downstream of the stent, points of zero wall shear stress correspond to flow separation and reattachment.

for both Newtonian and non-Newtonian flow. The plot only shows the shear stress over the last stent wire as well as within the region immediately downstream of the stent, and it demonstrates that the primary impact of the non-Newtonian properties is to reduce the size of the flow separation zone downstream of the stent by approximately 8%.

More Realistic Stent Structures

All the simulations thus far have been for stents whose wires have been idealized as a series of parallel rings that are positioned orthogonal to the main flow direction (see Fig. 1). Real stents are complex structures in which the wires may cross in elaborate fashions. Furthermore, stents from different manufacturers have markedly different designs. We have initiated efforts that aim to elucidate the impact of detailed stent design on the local hemodynamic environment in the vicinity of the stent. Toward this goal, we have constructed two computational models of geometries more representative of actual stents. The first is a stent consisting of a single 360° spiral with a pitch of approximately 7.5 mm and with a solid ring at the downstream end of the spiral (Fig. 11). Both the spiral and the ring have a $d/D = 0.1$. The second model consists of six intertwined rings that are formed by progressively rotating rings similar to those in Fig. 1 by angular increments of 30° and subsequently intertwining these rings (Fig. 12).

Our simulations on the spiral stent with a ring at its downstream end have revealed the presence of disturbed flow in the form of slowly moving streamlines immediately downstream of the ring that recirculate briefly prior to looping slowly in the forward direction. Figure 11 depicts the size of this disturbed flow zone (L/D) for two values of Re as a function of the angle around the ring (defined in Fig. 11). The results demonstrate that the size of the disturbed flow zone depends in a complex fashion on the angular position. Furthermore, the behavior at any angle depends on the Re. It should be noted that the different angles correspond to different distances from the body of the spiral, and this undoubtedly is an important consideration in dictating the size of the flow separation zone. We have also performed limited simulations on a stent consisting of three successive 360°-spirals with $d/D = 0.1$ and an interspiral spacing $w/D = 0.1$ and without a ring at its downstream end. The results in that case revealed the absence of flow recirculation downstream of the stent; rather, flow disturbance downstream of the stent took the form of forward-moving helical flow with no recirculation (data not shown).

Figure 12 depicts the magnitude of the wall shear rate in the vicinity of the six-ring intertwined stent. These results demonstrate that the shear rate varies locally over approximately three orders of magnitude. The lowest shear rates are generally present downstream of symmetric members of the stent, especially at strut-strut intersections (where two rings intersect). The shear rates downstream of asymmetric structures such as wires angled relative to the flow tend to be comparatively larger. These findings emphasize the great fluid mechanical heterogeneity that exists in the vicinity of complex stent geometries and point to the need for incorporating detailed stent design in studies of stent-induced fluid mechanical disturbance.

DISCUSSION

In this study, we have used CFD to investigate the flow field in the vicinity of endovascular stents positioned within straight and curved arterial segments. Of particular interest has been the impact of stent and vessel geometry as well as the flow conditions on the occurrence of flow disturbance, most notably flow separation and resultant recirculation. Disturbed flow has been implicated in the development of early atherosclerosis[3,23,25] and in neointimal formation in vascular grafts[32] and has been speculated to play a role in the development of instent restenosis.[7,37] The potential

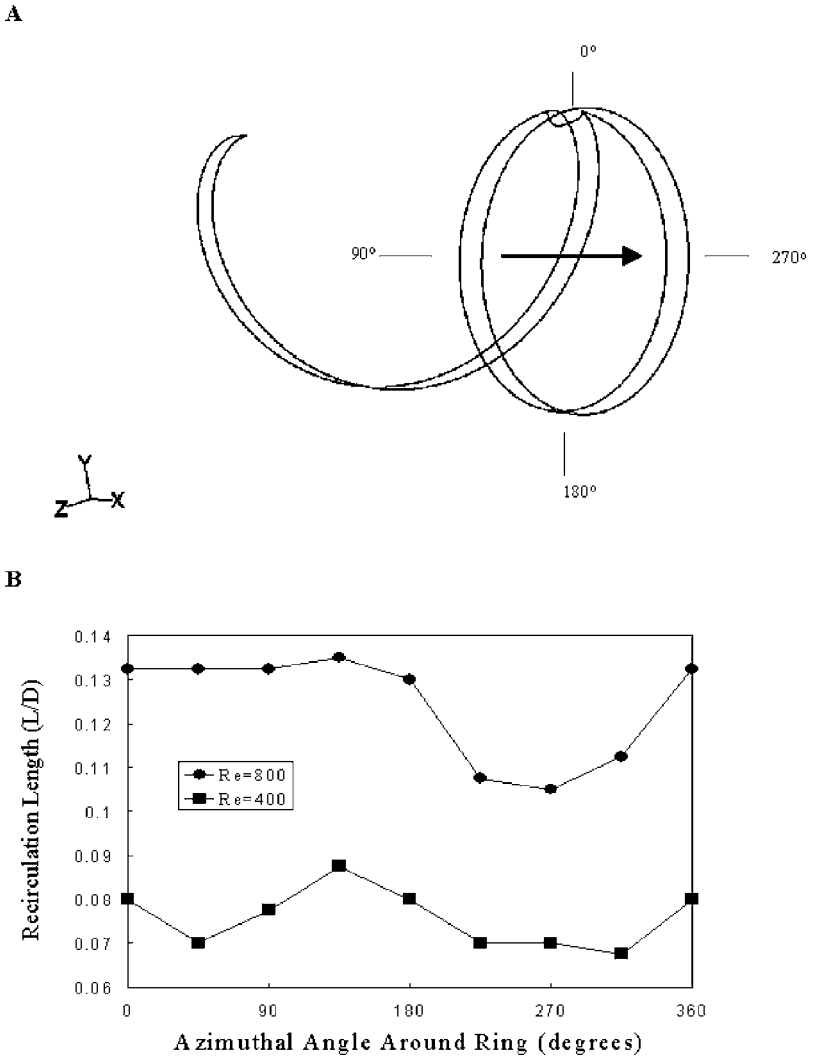

FIGURE 11. (A) Stent modeled as a single 360°-spiral with a ring attached to its downstream end. $d/D = 0.1$ for both the spiral and the ring. The angles shown denote the azimuthal angles around the ring perimeter. (B) Dependence of the size of the flow separation zone downstream of the ring on the azimuthal angle on the ring for steady flow with $Re = 400$ or 800.

role of fluid mechanical forces in restenosis may involve an effect of these forces on thrombus formation and activation shortly following stent deployment and/or an impact of flow on the rate of endothelial wound healing following stent-induced endothelial injury.

Our simulations have demonstrated that the presence of a stent within an arterial segment induces local disturbance in the flow field. This includes flow separation and recirculation between stent wires as well as upstream and downstream of the stent. As a result of this flow disturbance, the wall shear stress is elevated over the stent wires but is considerably lower in between wires and immediately downstream of the stent. This leads to large spatial gradients in wall shear stress within and around the stent. The size of the flow separation zone downstream of the stent depends in a complex fashion on the stent geometry and on the flow conditions. For instance, in straight vessel segments, the extent of flow separation downstream of the stent depends on both the stent wire thickness and the flow *Re*. For a given stent wire thickness, flow separation increases with *Re*, while for a given *Re*, separation increases with stent wire thickness but is relatively insensitive to the interwire spacing. Consistent with the previous results of Berry *et al.*,[7] the flow disturbance in between the stent wires is a strong function of the interwire spacing.

In curved vessels, the presence of a stent induces flow separation downstream of the stent both along the inner and outer walls of the curvature. However, the relative sizes of the flow separation zones along these two walls depend on both the flow *Re* and the angle of curvature. Wentzel *et al.*[37] noted that the outer wall in a curved stented vessel generally exhibits less neointimal hyperplasia than the inner wall, and these findings were used to argue that neointimal

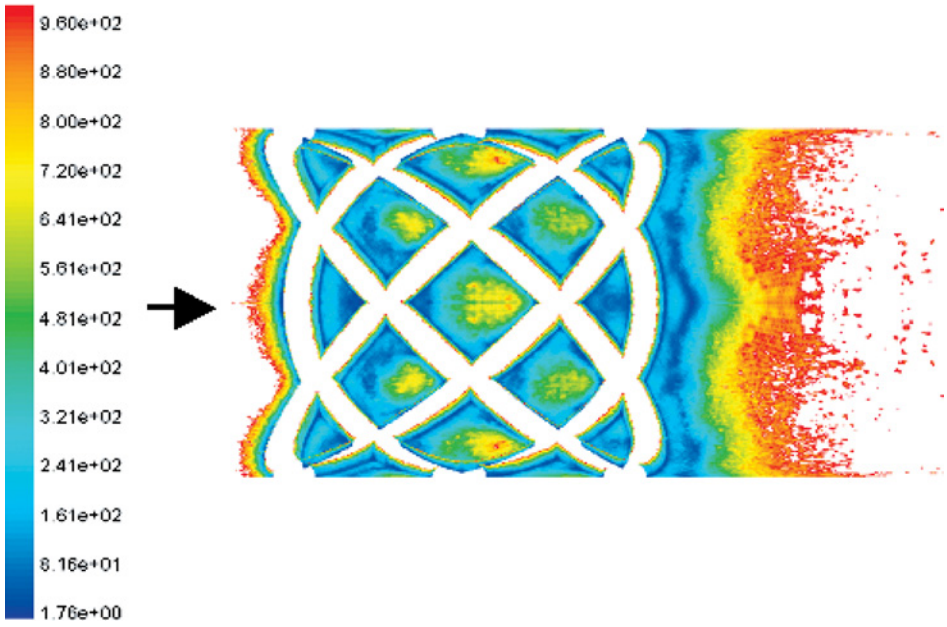

FIGURE 12. Magnitude of the wall shear rate (s^{-1}) in the immediate vicinity of a stent modeled as six intertwined rings with $d/D = 0.1$. Flow is steady with $Re = 400$. The arrow denotes the direction of flow.

hyperplasia correlates preferentially with regions of low wall shear stress. The present results suggest that in the presence of a stent, the relative magnitudes of the wall shear stress along the inner and outer walls of a curved arterial segment depend in a complex fashion on the vessel curvature and the *Re* and may be difficult to predict *a priori*.

Flow pulsatility leads to the periodic increase and decrease in the size of the flow separation zones downstream of stents in both straight and curved vessels. This leads to sizable temporal gradients in wall shear stress in addition to the large spatial gradients present in steady flow. Our results also demonstrate that the maximum size of flow separation zones downstream of stents positioned within straight vessel segments is equivalent for pulsatile flow to that for steady flow at the same cycle-peak *Re*. A phase lag exists between the flow rate and the size of the recirculation flow zone downstream of the stent. The phase lag observed ($\sim 30^\circ$) exceeds that predicted by Womersley theory alone ($\sim 16^\circ$), suggesting that the stent contributes to this phase lag. We have also conducted limited simulations in which the non-Newtonian behavior of blood has been taken into account. These simulations have revealed that while the non-Newtonian properties have a very limited impact on the global characteristics of the flow field, they do lead to a modest reduction in the size of the flow separation zone downstream of the stent.

Our simulations have revealed that the details of stent design have a major effect on the nature and extent of stent-induced flow disturbance. For instance, simulations performed on a model of a stent consisting of a spiral with a ring positioned at its downstream end have demonstrated a region of flow separation and reversal immediately distal to the ring. In contrast, a stent consisting of three successive 360°-spirals and without a ring at its downstream end exhibits no flow recirculation but rather local flow disturbance that takes the form of forward moving helical flow. These results emphasize the need for understanding the physics of stent–fluid interactions and highlight the notion that fluid mechanical analysis may be useful for the optimization of stent design in order to minimize the occurrence of stent-induced flow disturbance. Interestingly, recent clinical investigations have demonstrated that reduced stent strut thickness is associated with significant reduction in the incidence of restenosis[20] and that stent design plays an important role in the hyperplastic response of the vessel wall post stenting.[21]

Our simulations have assumed that both the arterial wall and the stent are rigid. Although advanced atherosclerosis leads to hardening of the arterial wall due to the formation of calcified plaque so that the compliance of the wall at the site of stent deployment is expected to be relatively low, it is important for future studies to probe the possible influence of wall motion, however limited, on the flow field in the vicinity of a stent. We have also assumed that stent placement does not alter the geometry of the vascular wall. There is evidence that upon deployment, stent struts commonly push against the arterial wall leading to local expansion in the vessel. Natarajan and Mokhtarzadeh-Dehghan[28] have performed simulations that have demonstrated that this alteration in local vessel geometry may lead to the formation of additional flow separation and recirculation zones.

Rogers and Edelman[33] investigated two different stent designs in rabbit iliac arteries and reported that reduction in the number of strut–strut intersections significantly reduces the incidence of thrombosis and neointimal hyperplasia. These observations are consistent with the notion advanced here that the details of stent design may impact the long-term prognosis for stent performance. More specifically, our findings suggest that regions downstream of strut–strut intersections exhibit relatively larger flow separation and recirculation zones. In conjunction with the present findings that the nature and extent of flow disturbance for a given stent design depends on the flow *Re* and the vessel geometry, this raises the intriguing possibility of tailoring stent design for implantation at specific vascular sites.

As pointed out elsewhere,[7] it is thought that the present simulations are most directly relevant to the acute situation in which thrombus formation occurs minutes following stent deployment. Stent overexpansion and neointimal tissue growth over time might be expected to alter the vessel geometry so that the chronic flow field in the vicinity of the stent might be different from the one described here. However, if the acute thrombotic response plays a role in determining the longer-term tissue response as has been suggested,[7,34] then our results may have important implications for the chronic response including the development of intimal hyperplasia and instent restenosis. Naturally, these complex processes involve activation of various biochemical pathways that the present study does not address and that should be probed in independent investigations.

In addition to its possible impact on instent thrombosis, the local fluid mechanical environment may also be involved in regulating vascular wound healing following endothelial injury induced by stent deployment. Research over the past two decades has established that fluid mechanical forces, particularly shear stress, intricately regulate the structure and function of vascular endothelial cells.[4,14,31] Of more direct relevance to the present work, shear stress has been shown to impact fundamental endothelial cell processes involved in wound healing including cell proliferation and migration. More recent data suggest that the endothelial cell responsiveness to shear stress depends on the precise character of the applied shear stress.[11,19,24,36] These observations, in combination with the present results demonstrating that different stent designs can lead to dramatically different types of flow disturbance, point to the possibility that stent design may be an important factor in determining the rate and extent of stent reendothelialization and hence potentially the likelihood of success of a stenting procedure.

ACKNOWLEDGMENTS

This work was supported in part by a grant from the Institute of Scientific Computational Research at the Lawrence Livermore National Laboratory. Dr. Seo was supported by the Professor Exchange Research Program of Andong National University and Brain Korea 21.

REFERENCES

[1] Albuquerque, M. L. C., C. M. Waters, U. Savla, H. W. Schnaper, and A. S. Flozak. Shear stress enhances human endothelial cell wound closure in vitro. *Am. J. Physiol.* 279:H293–H302, 2000.

[2] Armaly, B. F., F. Durst, J. C. F. Pereira, and B. Schonung. Experimental and theoretical investigation of backward-facing step flow. *J. Fluid Mech.* 127:473–496, 1983.

[3] Asakura, T., and T. Karino. Flow patterns and spatial distribution of atherosclerotic lesions in human coronary arteries. *Circ. Res.* 66:1045–1066, 1990.

[4] Barakat, A. I. Responsiveness of vascular endothelium to shear stress: Potential role of ion channels and cellular cytoskeleton. *Int. J. Mol. Med.* 4:323–332, 1999.

[5] Barakat, A. I., T. Karino, and C. K. Colton. Microcinematographic studies of the flow field in the excised rabbit aorta. *Biorheology* 34:195–221, 1997.

[6] Berger, S. A., L. Talbot, and L.-S. Yao. Flow in curved pipes. *Annu. Rev. Fluid Mech.* 15:461–512, 1983.

[7] Berry, J. L., A. Santamarina, J. E. Moore, Jr., S. Roychowdhury, and W. D. Routh. Experimental and computational flow evaluation of coronary stent. *Ann. Biomed. Eng.* 28:386–398, 2000.

[8] Caro, C. G. The Mechanics of the Circulation. Oxford: Oxford University Press, 1978.

[9] Carter, A. J., D. Scott, J. R. Laird, L. Bailey, J. A. Kovach, T. G. Hoopes, K. Pierce, K. Heath, K. Hess, A. Farb, and R. Virmani. Progressive vascular remodeling and reduced neointimal formation after placement of a thermoelastic self-expanding Nitinol stent in an experimental model. *Catheter. Cardiovasc. Diag.* 44:193–201, 1998.

[10] Chandran, K. B. Flow dynamics in the human aorta. *J. Biomech. Eng.* 115:611–616, 1993.

[11] Chappell, D. C., S. E. Varner, R. M. Nerem, R. M. Medford, and R. W. Alexander. Oscillatory shear stress stimulates adhesion molecule expression in cultured human endothelium. *Circ. Res.* 82:532–539, 1998.

[12] Cheer, A. Y., H. A. Dwyer, A. I. Barakat, E. Sy, and M. Bice. Computational study of the effect of geometric and flow parameters on the steady flow field at the rabbit aorto-celiac bifurcation. *Biorheology* 35:415–435, 1998.

[13] Chien, S., S. Usami, M. Taylor, J. L. Lundberg, and M. I. Gergersem. Effects of hematocrit and plasma proteins on human blood rheology at low shear rates. *J. Appl. Physiol.* 21:81–87, 1966.

[14] Davies, P. F. Flow-mediated endothelial mechanotransduction. *Physiol. Rev.* 75:519–560, 1995.

[15] Depaola, N., M. A. Gimbrone, Jr., P. F. Davies, and C. F. Dewey, Jr. Vascular endothelium responds to fluid shear stress gradients. *Arterioscler. Thromb.* 12:1254–1257, 1992.

[16] Emanuelsson, H., W. J. van des Giessen, and P. W. Serruys. Benestent II: Back to the future. *J. Intervent. Cardiol.* 7:587–592, 1994.

[17] Ettenson, D. S., E. W. Y. Koo, J. L. Januzzi, and E. R. Edelman. Endothelial heparan sulfate is necessary but not sufficient for control of vascular smooth muscle cell growth. *J. Cell. Physiol.* 184:93–100, 2000.

[18] Frank, A. O., P. W. Walsh, and J. E. Moore, Jr. Computational fluid dynamics and stent design. *Artif. Organs* 26:614–621, 2002.

[19]Helmlinger, G., B. C. Berk, and R. M. Nerem. Calcium responses of endothelial cell monolayers subjected to pulsatile and steady laminar flow differ. *Am. J. Physiol.* 269:C367-C375, 1995.

[20]Kastrati, A., J. Mehilli, J. Dirschinger, F. Dotzer, H. Schuhlen, F.-J. Neumann, M. Fleckenstein, C. Pfafferott, M. Seyfarth, and A. Schomig. Intracoronary stenting and angiographic results—Strut thickness effect on restenosis outcome (ISAR-STEREO) trial. *Circulation* 103:2816–2821, 2001.

[21]Kastrati, A., J. Mehilli, J. Dirschinger, J. Pache, K. Ulm, H. Schuhlen, M. Seyfarth, C. Schmitt, R. Blasini, F.-J. Neumann, and A. Schomig. Restenosis after coronary placement of various stent types. *Am. J. Cardiol.* 87:34–39, 2001.

[22]Komatsu, R., M. Ueda, T. Naruko, A. Kojima, and A. T. Becker. Neointimal tissue response at sites of coronary stenting in humans—Macroscopic, histological, and immunohistochemical analyses. *Circulation* 98:224–233, 1998.

[23]Ku, D. N., D. P. Giddens, C. K. Zarins, and S. Glagov. Pulsatile flow and atherosclerosis in the human carotid bifurcation: Positive correlation between plaque location and low and oscillating shear stress. *Arteriosclerosis* 5:293–302, 1985.

[24]Lum, R. M., L. M. Wiley, and A. I. Barakat. Influence of different forms of shear stress on vascular endothelial TGF-β1 mRNA expression. *Int. J. Mol. Med.* 5:635–641, 2000.

[25]Moore, J. E., C. Xu, S. Glagov, C. K. Zarins, and D. N. Ku. Fluid wall shear stress measurements in a model of the human abdominal aorta: Oscillatory behavior and the relationship to atherosclerosis. *Atherosclerosis* 110:225–240, 1994.

[26]Morice, M.-C., P. W. Serruys, J. E. Sousa, J. Fajadet, E. B. Hayashi, M. Perin, A. Colombo, G. Schuler, P. Barragan, G. Guagliumi, F. Molnar, and R. Falotico. A randomized comparison of a sirolimus-eluting stent with a standard stent for coronary revascularization. *N. Engl. J. Med.* 346:1773–1780, 2002.

[27]Moses, J. W., M. B. Leon, J. J. Popma, P. J. Fitzgerald, D. R. Holmes, C. O'Shaughnessy, R. P. Caputo, D. J. Keriakes, D. O. Williams, P. S. Teirstein, J. L. Jaeger, and R. E. Kuntz. Sirolimus-eluting stents versus standard stents in patients with stenosis in a native coronary artery. *N. Engl. J. Med.* 349:1315–1323, 2003.

[28]Natarajan, S., and M. R. Mokhtarzadeh-Dehghan. A numerical and experimental study of periodic flow in a model of a corrugated vessel with application to stented arteries. *Med. Eng. Phys.* 22:555–566, 2000.

[29]Nerem, R. M. Vascular fluid mechanics, the arterial wall, and atherosclerosis. *J. Biomech. Eng.* 114:274–282, 1992.

[30]Pedley, T. J. The Fluid Mechanics of Large Blood Vessels. Cambridge, UK: Cambridge University Press, 1980.

[31]Resnick, N., and M. A. Gimbrone, M. A., Jr. Hemodynamic forces are complex regulators of endothelial gene expression. *FASEB J.* 9:874–882, 1995.

[32]Rhee, K., and J. M. Tarbell. A study of the wall shear rate distribution near the end-to-end anastomosis of a rigid graft and compliant artery. *J. Biomech.* 27:329–338, 1994.

[33]Rogers, C., and E. R. Edelman. Endovascular stent design dictates experimental restenosis and thrombosis. *Circulation* 91:2995–3001, 1995.

[34]Rogers, C., S. Parikh, P. Seifert, and E. R. Edelman. Endogenous cell seeding—Remnant endothelium after stenting enhances vascular repair. *Circulation* 94:2909–2914, 1996.

[35]Schatz, R. A. A view of vascular stents. *Circulation* 79:445–457, 1989.

[36]Suvatne, J., A. I. Barakat, and M. E. O'Donnell. Shear stress regulation of endothelial Na-K-Cl co-transport expression: Dependence on K^+ and Cl^- channels. *Am. J. Physiol.* 280:C216–C227, 2001.

[37]Wentzel, J. J., R. Krams, C. H. Schuurbiers, J. A. Oomen, J. Kloet, W. J. van der Giessen, P. W. Serruys, and C. J. Slager. Relationship between neointimal thickness and shear stress after Wallstent implantation in human coronary arteries. *Circulation* 103:1740–1745, 2001.

[38]Wentzel, J. J., D. M. Whelan, W. J. van der Giessen, H. M. M. van Beusekom, I. Andhyiswara, P. W. Serruys, C. J. Slager, and R. Krams. Coronary stent implantation changes 3-D vessel geometry and 3-D shear stress distribution. *J. Biomech.* 33:1287–1295, 2000.

[39]White, C. R., M. Haidekker, X. P. Bao, and J. A. Frangos. Temporal gradients in shear, but not spatial gradients, stimulate endothelial cell proliferation. *Circulation* 103:2508–2513, 2001.